Targeting collagen strands by photo-triggered triple-helix hybridization

Yang Li[a], Catherine A. Foss[b], Daniel D. Summerfield[c], Jefferson J. Doyle[d], Collin M. Torok[b], Harry C. Dietz[d,e], Martin G. Pomper[b,f], and S. Michael Yu[a,c,f,1]

[a]Department of Chemistry, Johns Hopkins University, Baltimore, MD 21218; [b]Department of Radiology and Radiological Science, Johns Hopkins University School of Medicine, Baltimore, MD 21231; [c]Department of Materials Science and Engineering, Johns Hopkins University, Baltimore, MD 21218; [d]Howard Hughes Medical Institute and Institute of Genetic Medicine, Johns Hopkins University School of Medicine, Baltimore, MD 21205; [e]Division of Pediatric Cardiology, Department of Pediatrics, and Department of Medicine, Johns Hopkins University School of Medicine, Baltimore, MD 21205; and [f]Institute for NanoBiotechnology, Johns Hopkins University, Baltimore, MD 21218

Edited by* David A. Tirrell, California Institute of Technology, Pasadena, CA, and approved August 3, 2012 (received for review June 7, 2012)

Collagen remodeling is an integral part of tissue development, maintenance, and regeneration, but excessive remodeling is associated with various pathologic conditions. The ability to target collagens undergoing remodeling could lead to new diagnostics and therapeutics as well as applications in regenerative medicine; however, such collagens are often degraded and denatured, making them difficult to target with conventional approaches. Here, we present caged collagen mimetic peptides (CMPs) that can be photo-triggered to fold into triple helix and bind to collagens denatured by heat or by matrix metalloproteinase (MMP) digestion. Peptide-binding assays indicate that the binding is primarily driven by stereo-selective triple-helical hybridization between monomeric CMPs of high triple-helical propensity and denatured collagen strands. Photo-triggered hybridization allows specific staining of collagen chains in protein gels as well as photo-patterning of collagen and gelatin substrates. In vivo experiments demonstrate that systemically delivered CMPs can bind to collagens in bones, as well as prominently in articular cartilages and tumors characterized by high MMP activity. We further show that CMP-based probes can detect abnormal bone growth activity in a mouse model of Marfan syndrome. This is an entirely new way to target the microenvironment of abnormal tissues and could lead to new opportunities for management of numerous pathologic conditions associated with collagen remodeling and high MMP activity.

cancer | diagnostic imaging | connective tissue | degenerative disease | caged peptide

As the most abundant protein in mammals, collagens play a crucial role in tissue development and regeneration, and their structural or metabolic abnormalities are associated with debilitating genetic diseases and various pathologic conditions. Although collagen remodeling occurs during development and normal tissue maintenance, particularly for renewing tissues (e.g., bones), excess remodeling activity is commonly seen in tumors, arthritis, and many other chronic wounds. During collagen remodeling, large portions of collagens are degraded and denatured by proteolytic enzymes, which can be explored for diagnostic and therapeutic purposes. Since unstructured proteins are not ideal targets for rational drug design, library approaches have been employed to develop monoclonal antibody (1, 2) and peptide probes (3) that specifically bind to cryptic sites in collagen strands that become exposed when denatured. However, these probes suffer from poor pharmacokinetics (4), and/or low specificity, and binding affinity (5).

We envisioned that triple helix, the hallmark structural feature of collagen, could provide a unique targeting mechanism for the denatured collagens. The triple helix is nearly exclusively seen in collagens except as small subdomains in a few noncollagen proteins (6). Considering its striking structural similarity to the DNA double helix in terms of multiplex formation by periodic interchain hydrogen bonds along the polymer backbone (6), we thought that a small peptide sequence with strong triple-helix propensity could specifically recognize collagen sequence and hybridize to collagen strands by forming triple helix in a manner similar to DNA fragments or peptide nucleic acids binding to complementary DNA strands (7).

Previously, we discovered that small collagen mimetic peptides (CMPs, molecular weight: 2–3 kDa) capable of reversibly forming collagen triple helices are able to bind to type I collagen (8–11). Binding was observed only when CMPs [$(ProHypGly)_x$, $x = 6$, 7, and 10] in a thermally melted, single-strand form and not in folded trimeric form were allowed to fold by cooling in the presence of type I collagen fibers (9, 10). Although we observed apparent CMP binding to collagens at temperatures below collagen's T_m, the binding was significantly enhanced when hot CMP solution (typically above 70 °C) was applied to the collagen film. This suggested that the binding is facilitated by collagen denaturation, which could provide more open collagen strands that can hybridize the CMPs. However, we were unable to quantitatively assess the effects of collagen denaturation on CMP binding because it was impossible to decouple CMP melting from collagen denaturation. In addition, application of hot CMP solution was not compatible with in vivo and ex vivo collagen-targeting experiments. Therefore, we explored nonthermal means to control triple-helix folding and identified photo-caging as an ideal alternative.

In this article, we present the design and synthesis of a new caged CMP that can be photo-triggered to fold into triple helix. Using the new caged CMP, we compare the CMP's binding affinity to intact type I collagen and the same collagen denatured by heat or by matrix metalloproteinase (MMP) digestion, as well as study its stereo-selective hybridization mechanism. We further show that fluorescently labeled CMPs can be used in vivo to target and image denatured collagens in tissues undergoing remodeling, either due to normal renewal process (e.g., bones and cartilages) or pathologic conditions, such as tumor progression (e.g., prostate and pancreatic cancers) and musculoskeletal disease (e.g., Marfan syndrome).

Results and Discussion

Design and Photo-triggered Folding of the Caged Collagen Mimetic Peptide. In the collagen triple helix, small Gly residues are periodically located at every third position in each collagen strand to allow close packing of three protein chains in a right-handed twist (Fig. 1*A*) (12, 13). Mutations at even a single Gly position can

Y.L., C.A.F., M.G.P., and S.M.Y. designed research; Y.L., C.A.F., D.D.S., and C.M.T. performed research; J.J.D. and H.C.D. contributed reagent/analytical tools; Y.L., C.A.F., J.J.D., M.G.P., and S.M.Y. analyzed data; and Y.L., C.A.F., J.J.D., H.C.D., M.G.P., and S.M.Y. wrote the paper.

The authors declare no conflict of interest.

*This Direct Submission article had a prearranged editor.

[1]To whom correspondence should be addressed. E-mail: yu@jhu.edu.

This article contains supporting information online at www.pnas.org/lookup/suppl/doi:10.1073/pnas.1209721109/-/DCSupplemental.

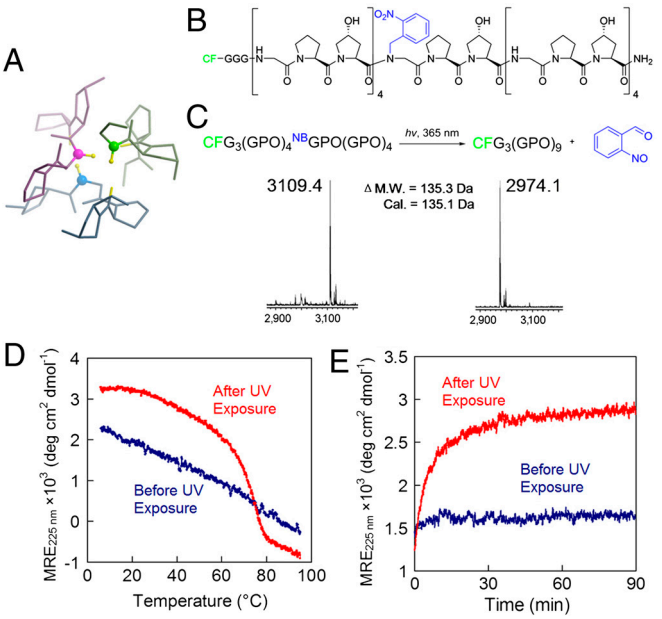

Fig. 1. Photo-triggered triple-helical folding of caged CMPs. (*A*) The backbone NH groups of Gly (represented by the ball-and-stick model) play a key role in stabilizing the collagen triple helix. (*B*) Structure of $CF^{NB}(GPO)_9$ featuring the photo-reactive nitrobenzyl (NB) group (in blue) conjugated to the central Gly. (*C*) Photo-cleavage of the NB cage group is monitored by MALDI-MS. (*D*, *E*) The NB cage group completely abolishes the triple-helical folding capacity of $CF^{NB}(GPO)_9$ and the photo-cleaving of the NB cage leads to CMP folding into stable triple helices, evidenced by CD melting studies (*D*) and refolding kinetics (*E*) of the peptides before and after UV exposure. For the refolding kinetic study (*E*), $CF^{NB}(GPO)_9$ (before and after UV exposure) were thermally quenched from 80 °C to 25 °C and the change in CD ellipticity at 225 nm was monitored at 25 °C.

destabilize the collagen structure and cause debilitating genetic disease (14). Therefore, we reasoned that a bulky, photo-cleavable cage group conjugated to the central Gly nitrogen of the CMP would fully negate its ability to fold (*SI Appendix*, Fig. S1), while exposure to light could liberate the cage group and trigger triple-helix folding and collagen binding. This approach was also appealing from a synthetic perspective as caged Gly, among all amino acids, is the easiest to synthesize and has the highest reactivity toward the addition of the next amino acid. The nitrobenzyl (NB) caged and carboxyfluorescein (CF) labeled CMP of sequence CF-Gly_3-$(GlyProHyp)_4$-^{NB}**Gly**ProHyp-$(GlyProHyp)_4$ [designated as $CF^{NB}(GPO)_9$, Fig. 1*B*] was synthesized by incorporation of Fmoc(N-*o*-nitrobenzyl)Gly-OH (15) during conventional Fmoc-mediated solid-phase peptide synthesis (SPPS). Coupling of Hyp to the sterically hindered ^{NB}Gly termini of the growing peptide was sluggish under HBTU/HOBT coupling condition; however, with the more powerful activating agent, PyBroP (16), we were able to achieve almost quantitative coupling efficiency and continue coupling the remaining peptide by SPPS, including the triple Gly spacer and the CF fluorescent tag (*SI Appendix, Materials and Methods*, Fig. S2) (17).

As we had anticipated, $CF^{NB}(GPO)_9$ exhibited photo-triggered triple-helix folding behavior (Fig. 1 *C*–*E*). The NB cage group completely suppressed the CMP's ability to fold into a triple helix as evidenced by the linear CD intensity decrease during melting (Fig. 1*D*, and *SI Appendix*, Fig. S3). Exposure to UV light (365 nm, approximately 10 mW/cm^2) efficiently cleaved the NB (Fig. 1*C*, and *SI Appendix*, Table S1) which allowed the CMP to regain its full triple-helical folding capacity as exhibited by the sigmoidal CD melting curve (heating rate: 60 °C/h) with T_m at 75 °C and fast refolding kinetics after thermal quenching from 80 °C to 25 °C (Fig. 1 *D* and *E*).

Photo-Triggered CMP-Collagen Hybridization. Using the new caged CMP, we were able to study comparative CMP binding toward intact and thermally denatured (gelatin) type I collagen because collagen denaturation could be completely decoupled from CMP melting. Photo-triggered binding affinity of the caged CMP was studied by applying $CF^{NB}(GPO)_9$ to a 96-well assay microplate coated with collagen/gelatin films, followed by UV (365 nm) exposure and measuring the fluorescence intensity of the collagen films after washing. While caged CMP binding (UV−) remained negligible on both collagen and gelatin substrates, photo-activated caged CMPs (UV+) exhibited binding to both substrates with the level of binding an order of magnitude higher for gelatin (Fig. 2*A*). These results indicate that CMP's triple helical folding is required for the binding, and collagen denaturation produces unfolded collagen strands that avidly hybridize with photo-decaged CMPs. The binding affinity was further confirmed for both type I and type II gelatin in comparison to sequence-scrambled CMPs which exhibited no triple-helical folding capacity (*SI Appendix*, Fig. S4) and negligible affinity to gelatin (Fig. 2*B*).

Although these experiments demonstrated collagen binding mediated by CMP's ability to fold into a triple helix, questions remain as to the precise mechanism underlying the CMP-collagen interactions. We addressed this question by studying the collagen affinity of a specially synthesized CMP composed of D-proline (^{D}P) which folds into an oppositely twisted left-handed triple helix. Since D-hydroxyproline is not readily available, we synthesized two caged Hyp-free CMPs; $CF^{NB}(GPP)_9$, which folds into a natural right-handed twist, and $CF^{NB}(G^{D}P^{D}P)_9$, which was expected to fold into an unnatural left-handed twist after photo-decaging. The CD melting curves of the two peptides after photo-cleavage were exact mirror images with identical T_m at 51 °C (*SI Appendix*, Fig. S5). Despite almost identical CD melting behaviors, $CF^{NB}(G^{D}P^{D}P)_9$ exhibited an order of magnitude lower levels of gelatin binding to that of $CF^{NB}(GPP)_9$ after photo-cleavage (Fig. 2*C*). Natural collagen strands can only fold into right-handed triple helices and are unlikely to form a triple-helical hybrid with a CMP having propensity for a left-handed twist (18). The results clearly show that the binding is not due to CMP trimers merely trapping the gelatin strands during triple-helical assembly, but that it is primarily driven by stereo-selective CMP-collagen strand hybridization, most likely in the form of a triple helix.

To investigate the low but apparent CMP-binding affinity to intact collagen films (Fig. 2*A*), we further performed a series of binding experiments using a noncaged, triple-helical $CF(GPO)_9$ and UV-triggered $CF^{NB}(GPP)_9/CF^{NB}(G^{D}P^{D}P)_9$ pair as well as thermally melted single-stranded $CF(GPO)_9$ (*SI Appendix, Text*, Figs. S6 and S7). The results confirm that CMP's binding affinity to intact type I collagen is real and also stereo-selective. We speculate that the low-level binding is caused by CMPs hybridizing with thermally unstable domains of the native collagen (19) or collagens partially denatured during purification and fiber regeneration. The density of photo-induced CMP binding to intact collagen was determined to be as high as 0.56 ± 0.03 $nmol/cm^2$, which is well above the bioactive ligand density for a variety of cell scaffold interactions in cell culture and tissue development (20, 21). Using $CF^{NB}(GPO)_9$, we were also able to photo-pattern collagen and gelatin films demonstrating the potential for local immobilization of CMP conjugated bioactive components (10, 22, 23) to collagen-containing tissue engineering scaffolds (Fig. 2*D*) (24, 25).

Since many pathologic conditions are associated with collagen remodeling by MMP activity, degraded collagens in diseased tissue and circulation are potential diagnostic and therapeutic targets (26, 27). Anti-collagen antibodies and low molecular weight targeting agents have been used to image collagens in fibrotic tissues and tumors, but they suffer from poor pharmacokinetics, and/or low specificity and binding affinity (2, 5). We tested the

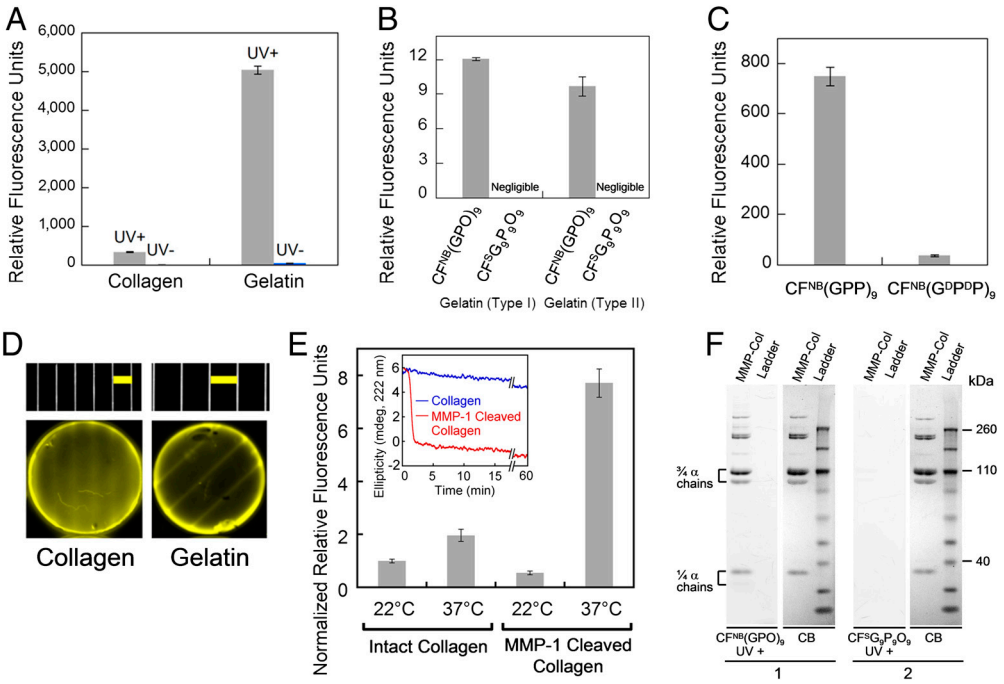

Fig. 2. Characterization of photo-triggered CMP-collagen hybridization. (*A*) Fluorescence levels of collagen films (fibrillar collagen) and thermally denatured collagen (gelatin) films treated by $CF^{NB}(GPO)_9$, with and without UV exposure. (*B*) Comparative fluorescence levels of type I and type II gelatin coatings treated with UV-exposed $CF^{NB}(GPO)_9$ and the sequence-scrambled control peptide, $CF^{S}G_9P_9O_9$ (CF-GGG-PGOGPGPOPOGOGOPPGOOPGGOOPPG). (*C*) Fluorescence levels of type I gelatin films treated with UV-exposed $CF^{NB}(GPP)_9$ and control peptide of opposite helicity, $CF^{NB}(G^DP^DP)_9$. (*D*) Fluorescence photographs of the photo-patterned collagen (*Left*) and gelatin (*Right*) films along with photographs of the transparency masks (*Top*, in scale with the photo-patterned films, *Below*) showing the line patterns [Scale bars: 2 mm (*Left*), 3 mm (*Right*)]. (*E*) Comparative fluorescence levels after photo-triggered $CF^{NB}(GPO)_9$ binding to nonfibrillar form of intact or MMP-1 cleaved type I collagens before and after 1 min of 37 °C incubation. *Inset*: CD signals after a temperature jump from 22 °C to 37 °C indicated fast denaturation (90% signal reduction in less than 3 min) of MMP-1 digested type I collagens at 37 °C while intact collagen maintained most of its triple-helical structure. (*F*) Fluorescence images of SDS-PAGE gels of MMP1-cleaved type I collagen (MMP-Col) and protein ladder stained with $CF^{NB}(GPO)_9$ (gel 1) or $CF^{S}G_9P_9O_9$ (gel 2) upon UV-activation, and white light photographs of the same gels stained with coomassie brilliant blue (CB). Bands labeled as 3/4α and 1/4α chains are MMP-1 digested collagen fragments. All CMP binding assays were performed in triplicate (±s.d.).

caged CMP [$CF^{NB}(GPO)_9$]'s photo-triggered binding affinity to type I collagen after MMP-1 digestion (*SI Appendix*, Fig. S8 for SDS-PAGE and CD characterization). MMP-1 cleaves the ¾ position of the collagen molecule, resulting in two collagen fragments with T_m around 34 °C that spontaneously denature at body temperature (Fig. 2*E*, *Inset*) (28). The photo-triggered CMP-binding assay was performed on intact and MMP-1 digested collagens before and after incubation at 37 °C. For intact collagens, the level of CMP binding was similarly low for the two temperature conditions. In contrast, MMP-1 digested collagens after the 37 °C incubation exhibited approximately four to tenfold higher levels of CMP binding compared to all other collagens tested (Fig. 2*E*). These results show that CMPs preferentially hybridize with MMP-1 digested collagens, which are spontaneously denatured at body temperature, over intact collagens. This hybridization was further verified by SDS-PAGE staining experiment. When used as a gel-staining agent, only the photo-cleaved CMP and not the scrambled control peptide was able to stain the MMP-1 digested collagen bands (Fig. 2*F*). No other bands from the protein ladder were stained by the CMP, which demonstrates its high binding specificity to collagen chains.

In Vivo Tumor Targeting by CMP Hybridization. To demonstrate CMP's ability to target pathologic tissues of high MMP activity, we performed an in vivo tumor-targeting experiment, using the same caged CMP conjugated to a near-infrared fluorophore (NIRF). Tumor progression involves proteolytic remodeling of the extracellular matrix (ECM) by various MMPs that results in the accumulation of stromal collagens with a unique structural and biochemical signatures (27, 29–31). We conjugated IRDye800CW (IR) to the N-termini of the caged CMP $^{NB}(GPO)_9$ and the scrambled peptide $^{S}G_9P_9O_9$ with flexible aminohexanoic acid (Ahx) spacers (*SI Appendix, Materials and Methods*, Fig. S9 for synthesis and CD melting curves). The NIRF-labeled CMPs were rapidly decaged under intense UV light (365 nm, >25 mW/cm^2) and immediately injected into the tail vein of mice bearing subcutaneous PC-3 prostate tumor xenografts. Considering the slow folding rate of the CMP triple helix (half time of CMP refolding is approximately 50 min) and the short time delay before the injection (<5 min), most of the CMPs were expected to enter the bloodstream in single-stranded form (32). Once in the blood, the CMP solution is diluted by a factor of 20, which results in dramatic reduction in the folding rate because of the third-order folding kinetics (33). Therefore, we expected that the single-stranded CMPs would be able to circulate the body and eventually bind to denatured collagen strands by triple-helical hybridization. Serial in vivo fluorescence imaging over four days indicated that the IR-Ahx-$(GPO)_9$ was able to permeate the tumor vasculature and accumulate at the tumor sites, whereas the scrambled sequence (IR-Ahx-$^{S}G_9P_9O_9$) lacking triple-helix folding capacity showed minimal accumulation at the tumor sites (Fig. 3*A* and *SI Appendix*, Fig. S10). Furthermore, coinjection of mice with MMPSense680™ (34), a fluorescent beacon for MMP activity, clearly showed the colocalization (in yellow) of MMP activity (in red) and CMP binding (in green) in the tumors 102 h after CMP injection (Fig. 3*B*). Ex vivo fluorescence microscopy of the tumor sections indicated that IR-Ahx-$(GPO)_9$ (in blue) was present near the CD31 positive perivascular tissue (in red) and colocalized in part with antibody for MMP-1 cleaved collagen fragments (in green) (Fig. 3*C*). This confirms that the tumor uptake was caused by CMP reaching the tumor via the blood vessels followed by binding to MMP digested collagens

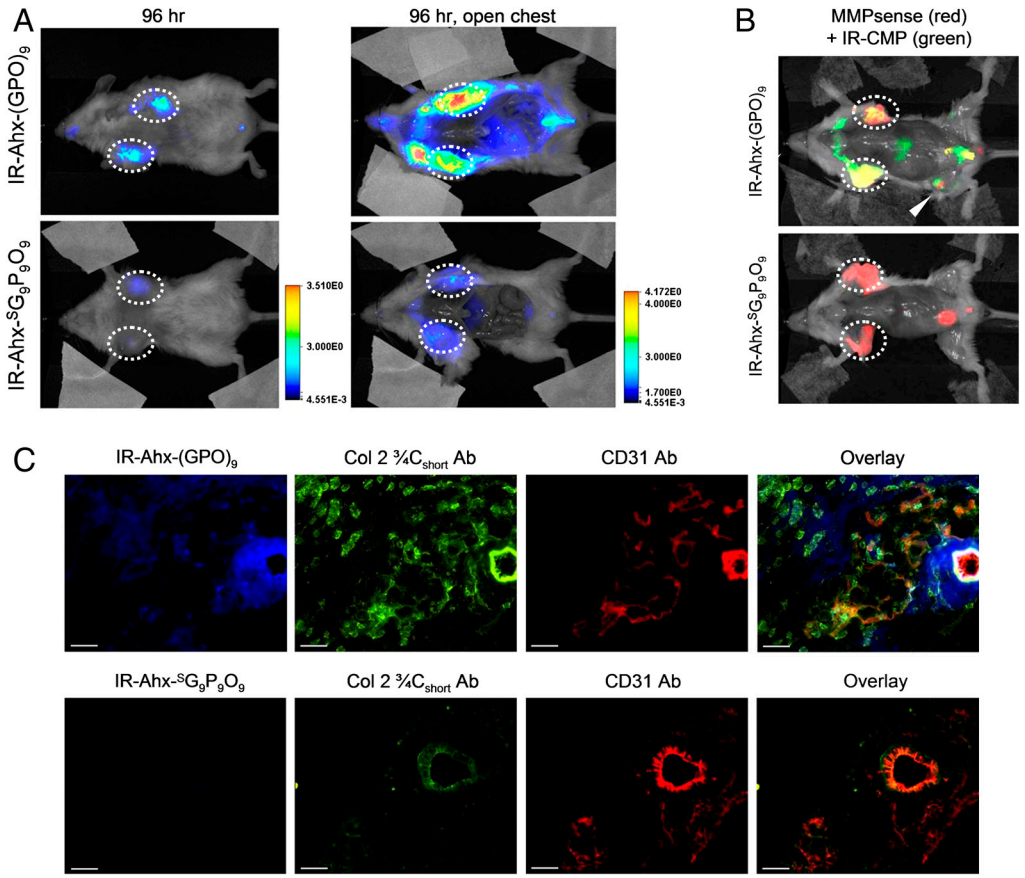

Fig. 3. In vivo targeting of tumors by CMP hybridization with MMP-digested collagens. (*A*) In vivo NIRF images of mice bearing PC-3 prostate tumors at forward right and left flanks (circled) administered with 3.7 nmol of UV-activated IR-Ahx-$^{NB}(GPO)_9$ or sequence-scrambled control peptide, IR-Ahx-$^{S}G_9P_9O_9$ via tail vein injection. Ventral views of both mice at 96 h post-injection (PI), and after midline surgical laparotomy (open chest) indicate tumor specific and stable accumulation of only the IR-Ahx-$(GPO)_9$ and not the control peptide. (*B*) NIRF images of another pair of mice bearing PC-3 tumors at the same location at 102 h after IR-CMP injection and 24 h after MMPSense680 injection, showing colocalization (in yellow) of MMP activity (red) and CMP binding (green) in the tumors (circled) and knee joint (arrowhead). (*C*) Epifluorescence micrographs of the unfixed PC-3 tumor sections from (*B*), additionally stained in vitro with anti-Col 2 ¾C_{short} csc antibody (green) and anti-CD31-PE antibody conjugate (red). IR-Ahx-$(GPO)_9$ (blue) colocalized partially with anti-Col 2 ¾C_{short} antibody (green) particularly within the peri-vasculatures. No such colocalization was detected for the control peptide (Scale bars: 100 μm).

within the tumor tissue. Similar results were obtained for mice bearing pancreatic tumor xenografts (*SI Appendix*, Fig. S11).

In Vivo Targeting of Collagen Remodeling in Bones and Cartilages. In both the prostate and pancreatic tumor targeting studies, we were surprised to see consistent and high level accumulation of CMPs at the knee joints, which also colocalized with MMP activity (Fig. 3*B*, and *SI Appendix*, Fig. S11*A*, arrowhead). Normal joints are known for continual tissue remolding by MMP; however, targeting this area by systemic delivery is difficult due to the avascular nature of the cartilage and fast synovial fluid clearance (35). To study the CMP accumulation at the joints and other tissues specifically, we conducted further in vivo CMP targeting experiments using BALB/c mice. This time, we used CMP conjugated to a slightly different NIRF dye, IRDye680RD (IR′) which has lower background fluorescence compared to 800CW. Fig. 4*A* shows the whole-body fluorescence image of the normal mouse four days after intravenous injection of the photo-decaged peptide. The images show clear accumulation of the CMPs within the skeleton, especially in the spine and ribs, as well as within the knees, ankles, wrists, and lower mandibles. Signals from other organs (harvested organs, *SI Appendix*, Fig. S12) were negligible except for the digestive system, which contained fluorescent chlorophylls from food (arrows). A mouse injected with sequence-scrambled peptide (IR′-Ahx-$^{S}G_9P_9O_9$) showed signal only from the digestive system. Furthermore, under similar experimental condition, neither the caged-CMP lacking the folding capacity nor the prefolded triple-helical CMP showed signs of skeletal uptake after four days (Fig. 4*B*). These results strongly suggest that the targeting of the skeletal tissue was mainly driven by the triple-helical propensity of the monomeric CMPs.

To identify the location of CMP binding more clearly, mice were coinjected with the calcium-chelating fluorescent probe (IRDye800CW BoneTag™) which targets calcifying tissues (36). Although the overall distributions of the two probes [IR′-Ahx-$(GPO)_9$: red; BonTag™: green] seemed similar (Fig. 4*C*, *Top*, and *SI Appendix*, Fig. S13*A*), close observation (Fig. 4*C*, *Bottom*, and *SI Appendix*, Fig. S13*B*) revealed that CMP targets both calcified and noncalcified bones (cartilages of the wrists, ribs, and knees) while the BoneTag™ targets only the calcified bones. The highest CMP intensity was detected at the articular cartilage of the knee joints (red arrow) sandwiched between two endochondral junctions (green arrows) targeted by both the BoneTag™ (green) and CMP (red). Ex vivo histologic analysis of the knee joint cartilage (unfixed frozen tissue section) showed CMP localizing at the superficial zone which was also costained by antibodies for MMP-1 cleaved, type II collagen fragments (Fig. 4*D*). The superficial zone is densely populated by type II collagen fibers, part of which are reported to be in denatured state due to steady remodeling activity (37). Because of continual bone remodeling, collagens within bone are metabolized throughout the lifespan, and products of collagen degradation (e.g., protein fragments, hydroxyproline) are markers for bone resorption activity (38). Considering the abundance of collagens in other organs, it is

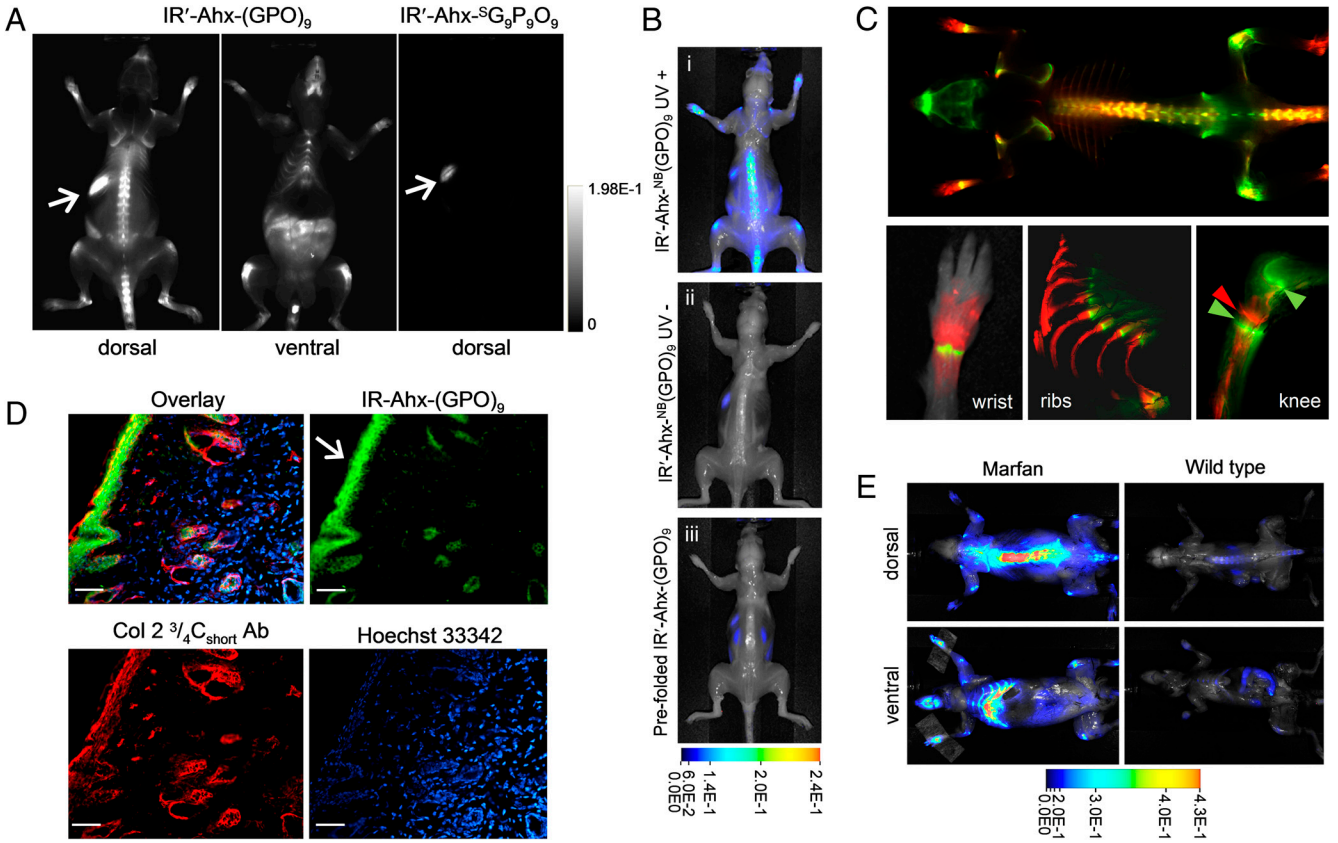

Fig. 4. In vivo targeting of collagen remodeling in bones and cartilages by CMP hybridization. (*A*) Whole-body NIRF images of BLAB/c mice injected intravenously with photo-decaged IR′-Ahx-$(GPO)_9$ or IR′-Ahx-$^{S}G_9P_9O_9$ showing skeletal uptake of only the IR′-Ahx-$(GPO)_9$ probes. Arrows show fluorescence from the chlorophyll in the digestive system. (*B*) Dorsal NIRF images of mice injected intravenously with photo-decaged IR′-Ahx-$(GPO)_9$ (*i*), caged IR′-Ahx-$^{NB}(GPO)_9$ (*ii*), or prefolded triple-helical IR′-Ahx-$(GPO)_9$ (*iii*). The absence of signal from mice *ii* and *iii* strongly suggests that the skeletal CMP uptake is due to its triple-helical folding propensity. (*C*) Dual-NIRF image of the whole skeleton showing the overall uptake of IR′-Ahx-$(GPO)_9$ (red) and BoneTag™ (stains calcifying tissues in green) and corresponding high-resolution images (colocalization shown in yellow). In the wrist, specific CMP uptake (red) is seen in carpal/metacarpal structures and BoneTag uptake is seen in epiphyseal line of radius and ulna; costochondral junctions within the ribs are visualized where mineralized bone ends (green-yellow) and cartilaginous ribs begin (red); CMPs colocalize with BoneTag™ at endochondral junctions (green arrowheads) in the knee while CMP-specific uptake can be seen within the articular cartilage and meniscus (red arrowhead) as well as focal regions within the tibia and the femur head. (*D*) Immunofluorescence micrographs of ex vivo knee cartilage sections subsequently stained with anti-Col 2 ¾C_{short} antibody and Hoechst 33342 showing high CMP accumulation at the superficial zone of the cartilage (Scale bars, arrow: 100 μm). (*E*) Whole-body NIRF images of mouse model with Marfan syndrome 96 h after IR′-Ahx-$(GPO)_9$ administration showing high CMP uptake in the skeleton of the diseased mouse. Whole body images were taken after skin removal.

remarkable to see such localized and apparently stable accumulation of CMPs in the bones and joints (little reduction in fluorescence intensity over 96 h). This suggests that the CMPs are preferentially hybridizing with denatured collagens within the tissue and not with collagen fragments in circulation which may be too small to fold into triple helix (10). These results suggest that the CMP could be used as cartilage-imaging agent, and appropriate derivatives may likewise become bone- and cartilage-seeking therapeutics. More work is under way to determine the effects of CMP hybridization on the process of collagen remodeling in the skeletal tissue and in tumor growth.

Finally, we tested CMP's potential to detect bone abnormality in a mouse model of Marfan syndrome, a genetic disorder of the ECM (39). Photo-triggered IR′-Ahx-$(GPO)_9$ was injected into mice with a heterozygous missense mutation in fibrillin-1, which was previously shown to exhibit marked skeletal pathology, including severe kyphosis (*SI Appendix*, Fig. S14) and rib overgrowth (39). Whole-body fluorescence images of the mutant and normal mice 96 h after the CMP injection showed a striking difference in CMP uptake: strong CMP signal was detected at the spine and ribs of the mutant mice with at least four times the intensity of the wild-type mice (Fig. 4*E*). The mechanism of bone overgrowth in Marfan syndrome is complex and still not fully understood; however, the strong correlation between collagen remodeling and bone growth in both physiological and pathological contexts (38), as well as high TGF-β signaling in multiple tissues of this mouse model support the conclusion that prominent CMP uptake in the Marfan mice, at least in part, derives from increased collagen remodeling in skeletal tissues that display pathological overgrowth.

More work is needed to fully understand the nature of CMP uptake in the skeletal tissues. The turnover rate of collagen in cartilages is reported to be significantly slower than that of the mineralized bones (40), and aortic aneurysm in Marfan disease is associated with an abnormally high concentration of mature collagens (41). Therefore, it is possible that the accumulation of degraded and damaged collagens, and not necessarily the fast rate of collagen degradation is responsible for the high CMP uptake seen in these tissues. It is also possible that calcification of collagens (i.e., mineralization) reduces CMP uptake. This could explain the high CMP uptake in the cartilage as well as the skeletal tissues of Marfan mouse which have reduced mineral content.

To our knowledge, this is the first time that the structural remodeling of ECM has been directly interrogated by peptide hybridization. CMP is a simple peptide that can be readily conjugated to imaging and therapeutic moieties. Therefore, CMP-mediated collagen strand targeting opens new avenues, beyond tumor, bone, and joint imaging, for applications in detection

and treatment of a wide range of pathologic conditions associated with high MMP activity, such as wound healing, ECM degeneration, and fibrous tissue formation.

Materials and Methods

Peptide Synthesis. Fmoc(N-*o*-nitrobenzyl)Gly-OH was synthesized as described in (15) (*SI Appendix*, Fig. S2*A*). Caged CMPs were coupled using standard solid-phase Fmoc and HBTU chemistry (10), with the exception of the amino acid following ^{NB}Gly, which was conjugated by 9 molar eq of the amino acid, 8.8 molar eq of PyBroP, and 20 molar eq of DIPEA for 24 h. The peptides were purified by reverse-phase HPLC and analyzed by MALDI-ToF (*SI Appendix*, Table S1) and circular dichroism spectroscopy.

Photo-Triggered Collagen Hybridization. Photo-triggered collagen binding studies were conducted by exposing CF-labeled, caged CMPs (50 μM or, as specified, 40 μL in 1 × PBS) to 365 nm UV light (10 mW/cm^2) directly on reconstituted type I collagen or gelatin films (0.742 mg of protein per film) at 4 °C, followed by 3 h of incubation, extensive washing, and fluorescence reading (ex: 489 nm; em: 533 nm). Type I collagen (416 μg/mL) was digested using MMP-1 (6.6 μg/mL) activated by p-aminophenylmercuric acetate. For comparative binding assays, wells of maxisorp microplates coated with intact and MMP-1 cleaved collagens (100 μg/mL) were blocked with 5% BSA and treated with CF^{NB}(GPO)$_9$ (20 μM; 50 μL in 1 × PBS), followed by UV exposure, incubation (2.5 h), extensive washing, and fluorescence reading.

In Vivo Tumor Targeting. All animal studies were undertaken in compliance with the regulations of the Johns Hopkins Animal Care and Use Committee. Prostate cancer cells (PC-3) were implanted (1 × 10^6 in 50 μL of HBS) subcutaneously behind the right and left forearms of non-obese diabetic (NOD)/severe-combined immunodeficient (SCID) mice. The tumors were grown until 5—7 mm in diameter, at which point, saline solution (100 μL) containing 3.7 nmol of IR-Ahx-^{NB}(GPO)$_9$ or IR-Ahx-^{S}G$_9$P$_9$O$_9$, and 1 nmol of cysteine (for quenching photo-cleaved aldehyde byproduct), activated by UV exposure (365 nm, >25 mW/cm^2, 5 min) was immediately injected via lateral tail vein. MMPSense 680™ (2 nmol in 150 μL 1 × PBS) was administered intravenously 80 h post CMP injection. Images were acquired at designated times using a LI-COR Pearl Impulse Imager at both 710 nm (MMPSense) and 800 nm (CMP). The unfixed tissue sections were probed with antibodies (anti-CD31, anti-Col 2 ¾C$_{short}$), followed by a secondary anti-rabbit-Alexa-Fluor488 and viewed using a Nikon 80i epifluorescence microscope.

In Vivo Skeleton Targeting. Male BALB/c mice (or Marfan mice developed as reported in ref. 39) were dosed with 4 nmol of UV-activated IR′-Ahx-^{NB}(GPO)$_9$ or IR′-Ahx-^{S}G$_9$P$_9$O$_9$ via tail vein as described. IRDye800CW BoneTag™ (10 nmol) was administered to each mouse 72 h post-CMP injection. After 24 h, the mice were imaged after their skins removed to allow imaging of deep tissues. Ex vivo hind limb and right hemisphere of ribs were scanned laterally using a LI-COR Odyssey imager in both 710 nm (CMP) and 800 nm (BoneTag) channels. For full detailed *Materials and Methods*, see *SI Appendix*.

ACKNOWLEDGMENTS. We thank Gilbert Green and Mrudula Pullambhatla for technical assistance, and Xuesong Jiang, Elena Makareeva, Robert Visse, and William Wilson for discussion. This work was supported by grants from NSF (DMR-0645411), NIAMS/NIH (R01-AR060484), and DOD awarded to S.M.Y., and from NIH (U24 CA92871 and U54 CA151838) awarded to M.G.P. Development and maintenance of Marfan mice was supported by NIH (AR-41135), the National Marfan Foundation, the William S. Smilow Center for Marfan Syndrome Research, and the Howard Hughes Medical Institute.

1. Pernasetti F, et al. (2006) Novel anti-denatured collagen humanized antibody D93 inhibits angiogenesis and tumor growth: An extracellular matrix-based therapeutic approach. *Int J Oncol* 29:1371–1379.
2. Xu J, Rodriguez D, Kim JJ, Brooks PC (2000) Generation of monoclonal antibodies to cryptic collagen sites by using subtractive immunization. *Hybridoma* 19:375–385.
3. Mueller J, Gaertner FC, Blechert B, Janssen K-P, Essler M (2009) Targeting of tumor blood vessels: A phage-displayed tumor-homing peptide specifically binds to matrix metalloproteinase-2-processed collagen IV and blocks angiogenesis in vivo. *Mol Cancer Res* 7:1078–1085.
4. Goldenberg DM (2002) Targeted therapy of cancer with radiolabeled antibodies. *J Nucl Med* 43:693–713.
5. Caravan P, et al. (2007) Collagen-targeted MRI contrast agent for molecular imaging of fibrosis. *Angew Chem Int Ed* 46:8171–8173.
6. Engel J, Bächinger HP (2005) *Collagen*, eds J Brinckmann, H Notbohm, and PK Müller (Verlag Berlin Heidelberg, Springer), pp 7–33.
7. Nielsen PE, Egholm M, Berg RH, Buchardt O (1991) Sequence-selective recognition of DNA by strand displacement with a thymine-substituted polyamide. *Science* 254:1497–1500.
8. Yu SM, Li Y, Kim D (2011) Collagen mimetic peptides: Progress toward functional applications. *Soft Matter* 7:7927–7938.
9. Wang AY, Mo X, Chen CS, Yu SM (2005) Facile modification of collagen directed by collagen mimetic peptides. *J Am Chem Soc* 127:4130–4131.
10. Wang AY, et al. (2008) Spatio-temporal modification of collagen scaffolds mediated by triple helical propensity. *Biomacromolecules* 9:1755–1763.
11. Li Y, Mo X, Kim D, Yu SM (2011) Template-tethered collagen mimetic peptides for studying heterotrimeric triple-helical interactions. *Biopolymers* 95:94–104.
12. Shoulders MD, Raines RT (2009) Collagen structure and stability. *Annu Rev Biochem* 78:929–958.
13. Fallas JA, O'Leary LER, Hartgerink JD (2010) Synthetic collagen mimics: Self-assembly of homotrimers, heterotrimers, and higher order structures. *Chem Soc Rev* 39:3510–3527.
14. Hyde TJ, Bryan MA, Brodsky B, Baum J (2006) Sequence dependence of renucleation after a Gly mutation in model collagen peptides. *J Biol Chem* 281:36937–36943.
15. Tatsu Y, Nishigaki T, Darszon A, Yumoto N (2002) A caged sperm-activating peptide that has a photocleavable protecting group on the backbone amide. *FEBS Lett* 525:20–24.
16. Nandy SK, Agnes RS, Lawrence DS (2007) Photochemically activated probes of protein-protein interactions. *Org Lett* 9:2249–2252.
17. Stahl PJ, Cruz JC, Li Y, Yu SM, Hristova K (2012) On-the-resin N-terminal modification of long synthetic peptides. *Anal Biochem* 424:137–139.
18. Punitha V, et al. (2009) Molecular dynamics investigations on the effect of D amino acid substitution in a triple-helix structure and the stability of collagen. *J Phys Chem B* 113:8983–8992.
19. Mo X, An YJ, Yun CS, Yu SM (2006) Nanoparticle-assisted visualization of binding interactions between collagen mimetic peptide and collagen fibers. *Angew Chem Int Ed* 45:2267–2270.
20. Anderson SM, Chen TT, Iruela-Arispe ML, Segura T (2009) The phosphorylation of vascular endothelial growth factor receptor-2 (VEGFR-2) by engineered surfaces with electrostatically or covalently immobilized VEGF. *Biomaterials* 30:4618–4628.
21. Rowley JA, Mooney DJ (2002) Alginate type and RGD density control myoblast phenotype. *J Biomed Mater Res* 60:217–223.
22. Chan TR, Stahl PJ, Yu SM (2011) Matrix-bound VEGF mimetic peptides: Design and endothelial cell activation in collagen scaffolds. *Adv Funct Mater* 21:4252–4262.
23. Wang AY, et al. (2008) Immobilization of growth factors on collagen scaffolds mediated by polyanionic collagen mimetic peptides and its effect on endothelial cell morphogenesis. *Biomacromolecules* 9:2929–2936.
24. Gillette BM, et al. (2008) In situ collagen assembly for integrating microfabricated 3D cell-seeded matrices. *Nat Mater* 7:636–640.
25. Nichol JW, et al. (2010) Cell-laden microengineered gelatin methacrylate hydrogels. *Biomaterials* 31:5536–5544.
26. Cretu A, Brooks PC (2007) Impact of the noncellular tumor microenvironment on metastasis: Potential therapeutic and imaging opportunities. *J Cell Physiol* 213:391–402.
27. Kessenbrock K, Plaks V, Werb Z (2010) Matrix metalloproteinases: Regulators of the tumor microenvironment. *Cell* 141:52–67.
28. Danielsen CC (1987) Thermal stability of human-fibroblast-collagenase-cleavage products of type-I and type-III collagens. *Biochem J* 247:725–729.
29. Liotta LA, et al. (1980) Metastatic potential correlates with enzymatic degradation of basement membrane collagen. *Nature* 284:67–68.
30. Conklin MW, et al. (2011) Aligned collagen is a prognostic signature for survival in human breast carcinoma. *Am J Pathol* 178:1221–1232.
31. Burns-Cox N, Avery NC, Gingell JC, Bailey AJ (2001) Changes in collagen metabolism in prostate cancer: A host response that may alter progression. *J Urol* 166:1698–1701.
32. Boudko S, et al. (2002) Nucleation and propagation of the collagen triple helix in single-chain and trimerized peptides: Transition from third to first order kinetics. *J Mol Biol* 317:459–470.
33. Ackerman MS, et al. (1999) Sequence dependence of the folding of collagen-like peptides. *J Biol Chem* 274:7668–7673.
34. Bremer C, Tung C, Weissleder R (2001) In vivo molecular target assessment of matrix metalloproteinase inhibition. *Nat Med* 7:743–748.
35. Rothenfluh DA, Bermudez H, O'Neil CP, Hubbell JA (2008) Biofunctional polymer nanoparticles for intra-articular targeting and retention in cartilage. *Nat Mater* 7:248–254.
36. Zaheer A, et al. (2001) In vivo near-infrared fluorescence imaging of osteoblastic activity. *Nat Biotechnol* 19:1148–1154.
37. Hollander AP, et al. (1995) Damage to type II collagen in aging and osteoarthritis starts at the articular surface, originates around chondrocytes, and extends into the cartilage with progressive degeneration. *J Clin Invest* 96:2859–2869.
38. Risteli J, Risteli L (2006) *Dynamics of Bone and Cartilage Metabolism*, eds MJ Seibel, SP Robins, and JP Bilezikian (Academic, New York) p 391.
39. Judge DP, et al. (2004) Evidence for a critical contribution of haploinsufficiency in the complex pathogenesis of Marfan syndrome. *J Clin Invest* 114:172–181.
40. Sivan S-S, et al. (2008) Collagen turnover in normal and degenerate human intervertebral discs as determined by the racemization of aspartic acid. *J Biol Chem* 283:8796–8801.
41. Lindeman JHN, et al. (2010) Distinct defects in collagen microarchitecture underlie vessel-wall failure in advanced abdominal aneurysms and aneurysms in Marfan syndrome. *Proc Natl Acad Sci USA* 107:862–865.